Revisiting Hurricane Track Model for Wind Risk Assessment

Reda Snaiki, Teng Wu*

Department of Civil, Structural and Environmental Engineering, University at Buffalo, Buffalo, NY 14126, USA

**Corresponding author. Email:* tengwu@buffalo.edu

Abstract: Hurricane wind risk assessment has been significantly improved with the evolvement of synthesis methodologies from the single site probabilistic method to the hurricane track model (including five simulation components of genesis, translation, intensity, decay and boundary-layer wind). As first-step efforts towards advancing the data-driven hurricane track model, widely used by engineering community, to a physics-based framework for more accurate and reliable hurricane risk assessment, a new intensity model integrating important dynamics and thermodynamics inside the storms is developed. Furthermore, an extensive statistical analysis of hurricane trajectories is carried out to obtain an enhanced translation model and a height-resolving analytical wind model is utilized to acquire the vertical profiles of wind speed and direction between ground-surface and gradient levels. The other two simulation components (i.e., genesis and decay) of the hurricane track model are also revisited for the sake of completeness. A 10,000 years of full-track synthetic hurricanes are generated and compared with the HURDAT database at specific mileposts along the US East coast to validate the overall performance of the developed simulation framework (in terms of annual occurrence rate, intensity, translation speed and heading angle). Then, the New Jersey coastline is employed as a case study to compare the simulated hurricane wind speeds with ASCE 7-16 recommendations, to highlight the wind directionality effects on extreme wind speeds, and to investigate the joint distribution of hurricane wind speed and size.

***Keywords*:** Hurricane track, Intensity model, Hurricane size, Wind directionality, Risk analysis.

1. Introduction

Hurricanes are among the most devastating natural hazards responsible for widespread damage to properties and life losses in the coastal regions due to their strong winds, torrential rainfall and storm surge [1, 2]. Despite the significant improvement in the hurricane hazard mitigation, recent events (e.g., Hurricane Katrina in 2005, Sandy in 2012 and Irma in 2017) have demonstrated that the coastal areas are highly vulnerable to landfalling hurricanes. The situation may become even worse with the increasing coastal population density, accelerated construction of infrastructures and changing climate [3-7]. Therefore, an effective engineering-based hurricane risk assessment tool that serves as the foundation for the risk mitigation, management and decision making in the hazard-prone regions is needed.

Early hurricane risk assessment based on the single site probabilistic simulation was pioneered by Russell [8, 9] and improved subsequently by other researchers [10-12]. Accordingly, the hurricane risk at the point of interest is obtained with the Monte Carlo technique sampling from site-specific statistical distributions of storm parameters, namely the central pressure deficit, radius of maximum winds, heading angle, forward speed, and coast crossing position. It is noted that the frequency of high-intensity events that significantly contribute to the hurricane risk analysis heavily depends on the tail shape of these assumed distribution, for which there is very little supporting data [13]. To overcome this limitation, Vickery et al. [14] introduced the hurricane track model to acquire the wind risk along the coastline of an entire continent based on statistics of a large amount of historical trajectory paths (including translation speed and direction) as well as the associated hurricane intensities. Since then, considerable efforts have been made to advance each simulation of hurricane track model [15-22]. Although the effectiveness of the statistical track generation in estimating the hurricane risk is well appreciated, the data-driven simulations of the hurricane intensity based on the statistics of historical records (e.g., linear statistical regression)

present weak robustness, poor interpolation and very limited predictability due to a lack of consideration of the underlying physics [23, 24]. To this end, Emanuel et al. [13] combined the statistical track generation with a physics-based, deterministic intensity modeling scheme for hurricane risk assessment. The coupled ocean-atmosphere model, with careful initialization, shows great promise in modeling the intensity evolution of storms along the tracks. However, the original construction of this physics-based intensity model cannot consider the important contribution from the environmental wind shear. To overcome this limitation, an empirical parametrization of shear effects is needed. It is noted that the modified hurricane intensity model with the consideration of wind shear effects is extremely sensitive to the initial conditions and several environmental factors that are currently poorly observed (e.g., middle tropospheric humidity) [23].

To facilitate the application of the statistical-deterministic methodology to hurricane risk assessment, a novel physics-based intensity model is developed in this study. The physics-based intensity model is simply governed by two mechanisms, namely a growth term representing the inward advection of angular momentum and a decay term through frictional forces that limit the intensity to an upper limit, and hence very convenient to be used together with the statistical track generator for hurricane risk assessment. In addition, an extensive statistical analysis of hurricane trajectories is carried out to obtain an enhanced translation model and a height-resolving wind model is utilized to acquire the vertical profiles of wind speed and direction between ground-surface and gradient levels. A 10,000 years of full-track synthetic hurricanes are generated and compared with the HURDAT database at specific mileposts along the US East coast to validate the overall performance of the developed simulation framework (in terms of annual occurrence rate, intensity, translation speed and heading angle). Then, the New Jersey coastline is employed as a case study to compare the simulated hurricane wind speeds with ASCE 7-16 recommendations, to

highlight the wind directionality effects on extreme wind speeds, and to investigate the joint distribution of hurricane wind speed and size.

2. Hurricane Track Model

The hurricane track model enhanced by the statistical-deterministic methodology can be employed to simulate the storm spatial and temporal evolutions from the initial to termination stages [13, 14, 25-28]. While the intensity as well as translation and boundary-layer wind simulation components will be highlighted in this study, other two components characterizing hurricane genesis and decay will also be briefly reviewed for the sake of completeness. The five modules of the hurricane track model, namely hurricane genesis, translation, intensity, decay and boundary-layer wind simulations as presented in Fig. 1 will be revisited in the following sections sequentially.

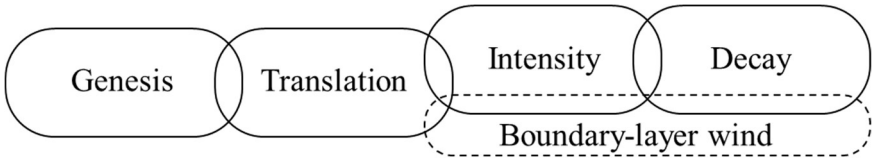

Fig. 1. Five simulation components of hurricane track model

2.1 Genesis model

The Hurricane Database version-2 (HURDAT2) provided by the National Hurricane Center contains the most updated hurricane tracks and environmental parameters since 1851 for the Atlantic and eastern north Pacific basins [29, 30]. Each hurricane track record provides the storm center initial location (in latitude and longitude coordinates) as well as the translational speed, heading angle and intensity every 6 hours [29, 30]. Fig. 2 presents the hurricane genesis locations for the Atlantic basin contained in the HURDAT2 database from which the initial condition of each simulated scenario is randomly selected. The historical annual hurricane frequencies from 1851-2016 are depicted in Fig. 3(a). In this study, the number of hurricanes per year is generated according to a negative binomial distribution $\mathrm{NB}(p,r)$ fitted to the HURDAT2 database [6, 7, 14,

18, 25-28, 31, 32], where p is the probability of success and r is the number of success. The parameters p and r of the negative binomial distribution are found to be 0.3709 and 6.5142, respectively, using the maximum likelihood estimation based on the historical records from 1851 to 2016. It can be seen from Fig. 3(b) that the obtained negative binomial distribution fits reasonably well with observation data.

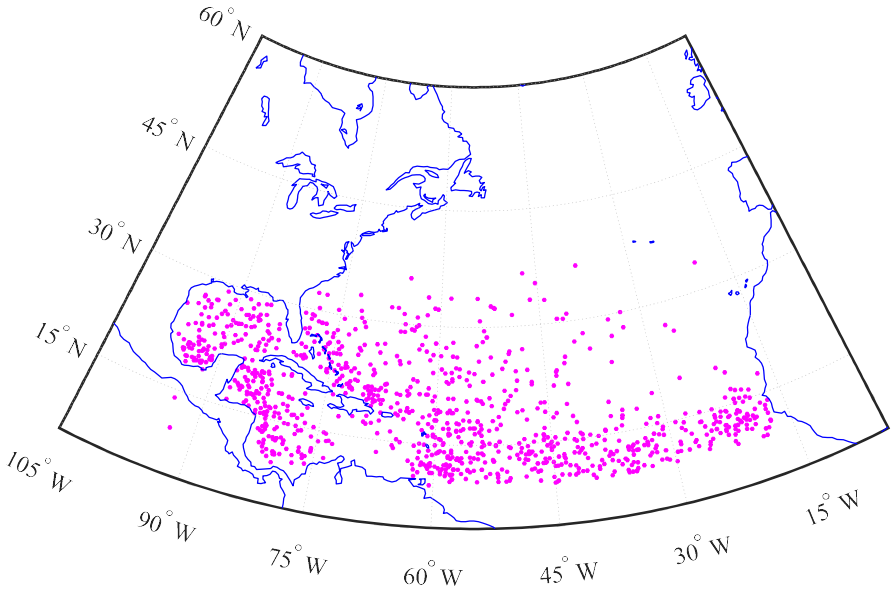

Fig. 2. Initial positions of historical hurricanes in HURDAT2 database

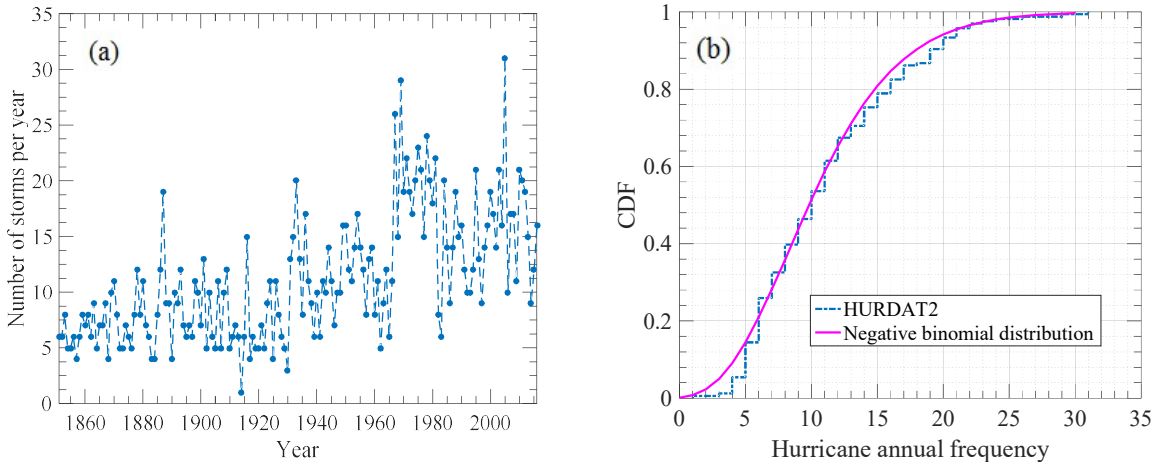

Fig. 3. Historical hurricanes in Atlantic basin: (a) Annual hurricane frequency; (b) Cumulative distribution of hurricane number per year

2.2 Translation model

The simulation of hurricane trajectories is based on the statistics of translation speed and heading angle (translation direction) obtained from the HURDAT2 6-hourly best track observations within each 5°x5° grid square, and the simulation domain is selected to be a region of North Atlantic bounded by 10N˚ to 60N˚ for the latitude and 0˚ to 110W˚ for the longitude [6, 7, 25-28, 32]. It should be noted that the main purpose of the translation model is designed for statistical track generation (without bias) but not for track forecasting [13]. Hence, there may exist a set of plausible translation models that perform well. Emanuel et al. [13] demonstrated that there is a nearly linear relationship between current and previous translation speeds and directions. Accordingly, only linear statistical models are considered here. While Emanuel et al. [13] indicated the evolution of hurricane trajectory path may be well described by Markov Chains, Zhang and Nishijima [24] showed the current translation speed and direction actually depend on the hurricane status of previous two time intervals (6 hours for each). In addition, Vickery et al. [14] presented that the hurricane translation speed and direction are not only dependent on each other, but also location dependent. Based on the abovementioned observations, three plausible statistical models for both translation speed (c) and direction (θ) are tested here. They are expressed as:

$$c_{i+1} = a_1 + a_2 c_i + \varepsilon \tag{1a}$$

$$c_{i+1} = a_1 + a_2 c_i + a_3 c_{i-1} + \varepsilon \tag{1b}$$

$$c_{i+1} = a_1 + a_2 c_i + a_3 \psi_i + a_4 \lambda_i + a_5 \theta_i + \varepsilon \tag{1c}$$

$$\theta_{i+1} = b_1 + b_2 \theta_i + \varepsilon \tag{2a}$$

$$\theta_{i+1} = b_1 + b_2 \theta_i + b_3 \theta_{i-1} + \varepsilon \tag{2b}$$

$$\theta_{i+1} = b_1 + b_2 \psi_i + b_3 \lambda_i + b_4 c_i + b_5 \theta_i + b_6 \theta_{i-1} + \varepsilon \tag{2c}$$

where a_j and b_j ($j = 1,...,6$) are regression constants to be determined for each 5° by 5° grid in

the simulation domain; i indicates the time step; ψ_i = hurricane eye latitude; λ_i = hurricane eye longitude; and ε = random error term.

The goodness-of-fit of the plausible statistical models is investigated through the corrected Akaike Information criterion (cAIC) defined as [33, 34]:

$$\mathrm{cAIC} = 2k - 2\ln(L) + \frac{2k^2 + 2k}{n - k - 1} \tag{3}$$

where k = number of estimated parameters; L = value of the maximum likelihood function for the model; and n = sample size. The cAIC favors the model with a smaller value, and hence offers a mean for model selection. In this study, it is used for eastward and westward directions separately, as shown in Figs. 4(a) and 4(b). As indicated in Fig. 4, the statistical model corresponding to Eq. (1c) is best suited for the translational speed simulation for the eastward case while Eq. (1a) should be selected for the westward case. On the other hand, more grids favor Eq. (2c) for the translation direction (heading angle) simulation for both eastward and westward cases.

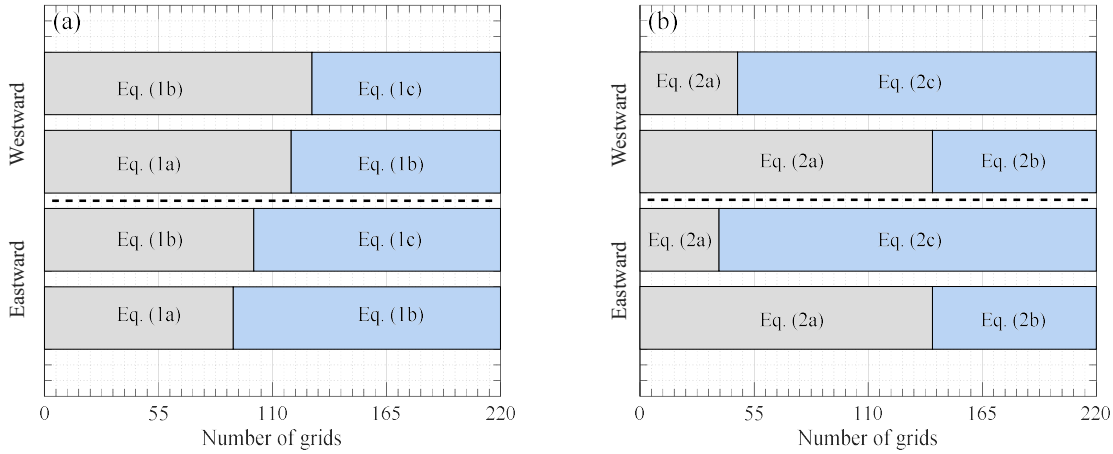

Fig. 4. Histograms of the number of grids with smaller cAIC values: (a) translational speed; (b) translation direction

2.3 Intensity model

Due to the extreme complexity of hurricanes, many models used by NHC as guidance in the preparation of official intensity forecasts are statistically based, e.g., the Statistical Hurricane

Intensity Prediction Scheme (SHIPS) developed by DeMaria et al. [35]. As a linear regression model, SHIPS characterizes the hurricane intensity as a linear function of a set of input parameters (predictors). The essential way to improve its robustness is by adding new predictors that may be important representatives of environmental factors. However, further improvements of SHIPS may be limited by the underlying linear nature of this regression model [36]. In addition, the relatively high number of input variables of SHIPS makes it not easy to be implemented in the context of hurricane risk assessment. Although DeMaria [36] further developed a logistic growth equation-based intensity model to significantly reduce the predictors by just considering the most important dynamic and thermodynamic properties, this simplified hurricane intensity is still empirically based. For the engineering applications, Vickery et al. [14] minimized the needed predictors by proposing an empirical intensity model in terms of relative intensity I, defined by Darling [37] as the actual central pressure drop normalized by the greatest possible central pressure drop that mean seasonal climatic conditions allow. It is noted that the latter depends on a number of thermodynamic factors, e.g., sea surface temperature (SST), relative humidity and temperature at the top of troposphere [6, 7, 25-28, 32].

Since the introduction of relative intensity factors out the SST effects on the hurricane intensity in terms of central pressure drop, a weak correlation is identified between SST and relative intensity [14]. However, SST is still explicitly retained in the model of Vickery et al. [14] to reduce some of the unexplained variance in the simulation process. Figure 5 presents the cAIC results with and without consideration of SST for the eastward and westward cases using HURDAT2 database, where α_j ($j=1,...,4$) is regression constant and T_i is SST at time step i. As shown in the figure, more grids are in favor of not including SST in the linear regression model of relative intensity for the case of Atlantic basin. Similar conclusion was obtained by Zhang and Nishijima [24] for the case of Northwest Pacific basin using the historical data from the Japan

Meteorological Agency (JMA).

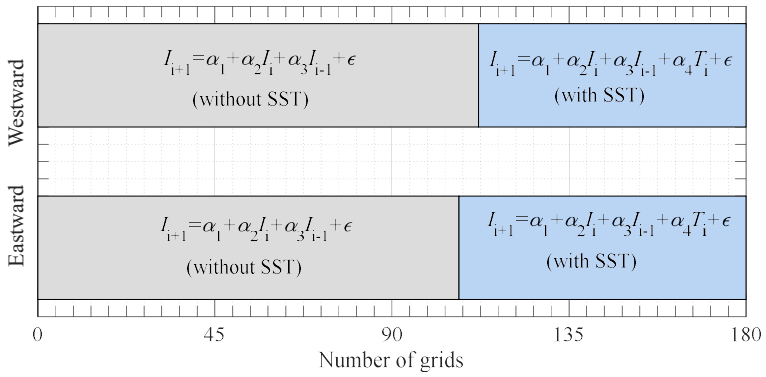

Fig. 5. Histogram of the number of grids with smaller cAIC values for hurricane intensity

To facilitate the development of a physics-based intensity model with relatively small number of predictors, the hurricane intensity simulation will be discussed in terms of the maximum sustained surface wind speed (at 10 m height) normalized by the maximum storm intensity V_{mpi}. It is noted that the inclusion of V_{mpi} in the hurricane intensity modeling highlights that the maximum sustained surface wind speeds are actually bounded by physical constraints [36, 38]. A widely-used formula characterizing V_{mpi} over the North Atlantic basin is expressed as [39]:

$$V_{mpi} = A' + B' e^{C'(T-T_0)} \tag{4a}$$

where T is the SST; T_0 is a specified reference temperature; A', B' and C' are constants to be determined by a least square fit. Several sets of constant values are obtained and used in Eq. (4a) to describe the relationship between V_{mpi} and SST [39-41], as presented in Fig. 6. The observed data based on all hurricanes of the North Atlantic basin (blue dots in Fig. 6) indicate V_{mpi} tends to level off for SST higher $28°\mathrm{C}$, however, this phenomenon cannot be well captured by Eq. (4a). To this end, a modified formula is proposed here as:

$$V_{mpi} = d + C_1 \exp\left[-C_2\left(T_0 / T\right)^{C_3}\right] \tag{4b}$$

where $T_0 = 28°\mathrm{C}$ and the constants are given by $d = 34.58\,m/s$, $C_1 = 80.41\,m/s$, $C_2 = 0.71$ and $C_3 = 5.09$ using a least square fit based on the HURDAT2 database. As shown in Fig. 6, the modified formula for V_{mpi} perform better than Eq. (4a) especially for high SST scenarios.

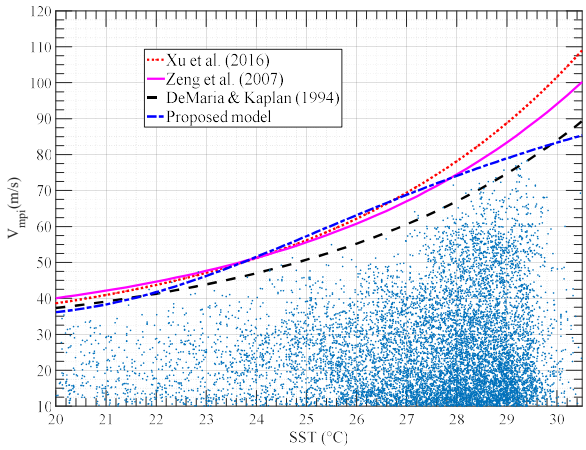

Fig. 6. Maximum storm intensity as a function of SST

In this study, the hurricane intensity evolution is explored using the Navier-Stokes equation for momentum in terms of v/V_{mpi} (denoted as V), where v is the azimuthal wind component. Accordingly, a first-order differential equation for the normalized intensity V in the cylindrical coordinate system (r,θ,z) can be obtained as:

$$\frac{\partial V}{\partial t} + u\frac{\partial V}{\partial r} + \frac{V \cdot V_{mpi}}{r}\frac{\partial V}{\partial \theta} + w\frac{\partial V}{\partial z} + \frac{uV}{r} + \frac{fu}{V_{mpi}} = \frac{F_{friction}}{V_{mpi}} \tag{5}$$

where u and w are radial and vertical wind components; the frictional force term $F_{friction}$ is represented through the bulk aerodynamic representation by $F_{friction} = -C_D v^2 / z_m$ (C_D = sea surface exchange coefficient for momentum and z_m = dimensional constant); the Coriolis force term fu/V_{mpi} can be disregarded since its contribution is insignificant compared to that of the centrifugal force [42]. In addition, the convective term $w(\partial V/\partial z)$ can be ignored as the vertical wind speed is negligible at the surface [42, 43]. To solve Eq. (5) for $V_{\max}$, the gradients of $\partial V_{\max}/\partial r$ and $\partial V_{\max}/\partial \theta$

are by definition equal to zero. Although an entirely different approach is used here, the obtained hurricane intensity model is governed by a differential equation similar to the logistic growth equation discussed in [36]. Accordingly, the dimensionless hurricane intensity is given by:

$$\frac{\partial V_{\max}}{\partial t} = \kappa V_{\max} - \beta' V_{\max}^2 \tag{6}$$

where $\kappa = \left(-u_m / R_{\max}\right)$ (u_m = radial wind speed associated to $V_{\max}$ and $R_{\max}$ = radius of maximum winds) and $\beta' = C_D V_{mpi} / z_m$. It should be noted that the upper limit of $V_{\max}$ governed by Eq. (6) is κ/β'. Accordingly, the hurricane intensity $v_{\max}$ is bounded by $(\kappa/\beta')V_{mpi}$ and controlled by two competing mechanisms, namely a growth term through the inward advection of angular momentum and a decay term through the friction. Both dynamic and thermodynamic factors affect the growth rate κ. DeMaria [36] proposed a new way to acquire κ as $a_1 S + a_2 C + a_3 SC + b$, where S is the 850-200 hPa vertical shear, C is the convective instability, and a_1, a_2, a_3 and b are constants to be determined. Substituting Eq. (4b) into Eq. (6), the hurricane intensity can be expressed as:

$$\frac{\partial V_{\max}}{\partial t} = \left(a_1 S + a_2 C + a_3 SC + b\right) V_{\max} - \beta \left[34.58 + 80.41 \mathrm{e}^{-\left(1.65*10^7\right)/T^{5.09}} \right] V_{\max}^2 \tag{7}$$

The vertical shear S is the magnitude of the 850-200-hPa vector difference, where the winds at 850 and 200 hPa are averaged over a circular area centered on the storm with a radius of 500 km; the convective instability C is the averaged vertical velocity of a parcel of air lifted from the surface to 15 km [44]; the sea surface temperature T at a 1° spatial resolution is available according to [45]; and $\beta' = \beta V_{mpi}$. Although the sea surface exchange coefficient that increases with wind speed up to $30\,m/s$ and then levels off has been investigated in detail by [46], its contribution to the hurricane intensity [represented by β in Eq. (7)] will be obtained through data in this study. The constant coefficients in Eq. (7) are determined based on 33 hurricanes that occurred between 2001

and 2016, and given by $a_1 = -0.0036\,h^{-1}$, $a_2 = 0.0040\,h^{-1}$, $a_3 = 0.0003\,h^{-1}$, $b = 0.0108\,h^{-1}$ and $\beta = 0.0004\,m^{-1}h^{-1}s$. The quality of the hurricane data used for model parameter estimation is carefully examined in this study. In addition, hurricanes without readily available environmental factors (e.g., vertical wind shear) or undergoing extratropical transition are excluded. The selected 33 hurricanes cover a wide range of storm characteristics (including various hurricane intensities). However, it should be noted that the identified parameters can be further refined with additional reliable hurricane data. It is noted that these coefficients present slight dependence on individual hurricanes, as also noticed by [36]. To solve for the hurricane intensity based on Eq. (7), the forward-time-differencing scheme is utilized that will provide the hurricane intensity at the 10-m height along the storm track. Regression analysis can be also performed using Eq. (7) fitted to the historical data of each grid.

2.4 Decay model

For the sake of completeness, the decay model of [47-49] utilized in this study is briefly summarized in this section. The evolution of the hurricane intensity [at 10-m height] after making landfall is determined as:

$$\frac{dv_{\max}}{dt} = -\mu\left(v_{\max} - v_b\right) \tag{8}$$

where v_b = background wind; and μ = decay constant. Equation (8) can be solved analytically leading to the following solution:

$$v_{\max}(t) = v_b + \left(v_{\max,o} - v_b\right)\exp(-\alpha t) \tag{9}$$

where $v_{\max,o}$ = initial intensity before landfall.

2.5 Boundary-layer wind model

An efficient and accurate hurricane boundary-layer wind model is needed to be coupled with the abovementioned track model for wind risk assessment. In most of engineering applications, the gradient wind speed v_g is first evaluated according to Georgiou [50]. Then, the surface wind speed v_{10} (at a standard reference height of 10 m above the ground) is obtained through a gradient-to-surface wind speed conversion factor that may present significant spatial variability. It should be noted that the wind direction is an important factor in the wind design for structures and usually not considered in such a wind simulation. In this study, the vertical profiles of both hurricane boundary-layer wind speed and direction between ground-surface and gradient levels will be simulated using a decomposition scheme [51, 52]. Accordingly, the hurricane boundary-layer wind velocity $(\boldsymbol{v})$ is expressed as:

$$\boldsymbol{v} = \boldsymbol{v}_g + \boldsymbol{v}' \tag{10}$$

where $\boldsymbol{v}_g$ = gradient wind in the free atmosphere; and $\boldsymbol{v}'$ = frictional component near the ground surface. The azimuthal wind speed at the gradient level could be straightforwardly solved in the cylindrical coordinate system as [43, 50]:

$$v_{\theta g} = \frac{\left(-c\sin\left(\theta-\upsilon\right)-fr\right)}{2} + \sqrt{\frac{\left(-c\sin\left(\theta-\upsilon\right)-fr\right)^2}{4} + \frac{B\Delta p}{\rho e}\left(\frac{R_{\max}}{r}\right)^B \exp\left[-\left(\frac{R_{\max}}{r}\right)^B\right]} \tag{11}$$

where υ = approach angle (counter clockwise positive from the East); c = hurricane translational speed; r = radial distance from hurricane center; θ = azimuthal angle; and Δp = central pressure difference. The radius of maximum winds $R_{\max}$ can be determined based on the following empirical formula [53]:

$$\ln\left(R_{\max}\right) = 3.015 - 6.291\times10^{-5}\Delta P^2 + 0.0337\psi + \varepsilon \tag{12}$$

The Holland parameter B over ocean is given by $B = 1.7642 - 1.2098\sqrt{A} + \varepsilon$ [53], where

$A = R_{\max} f \Big/ \sqrt{2R_d T \ln\left(1 + \frac{\Delta p}{p_c e}\right)}$ with the gas constant of dry air R_d and the central pressure p_c. After landfall, the Holland parameter is determined as $B(t) = B_0 \exp(at)$ where $a = 0.0291 - 0.0429 B_0$ and B_0 is the Holland parameter value at landfall. The radial wind component $v_{rg} = -\frac{1}{r}\int_0^r \frac{\partial v_{\theta g}}{\partial \theta} dr$ obtained from the continuity equation is usually insignificant and hence disregarded here [43].

To obtain the frictional component, the horizontal momentum equations are first simplified using the scale analysis approach, and then linearized leading to the following frictional wind speed formulas as [51, 52]:

$$u'(\theta, z') = (\alpha/\beta_a)^{1/2} \times Real\left\{A_0 \times e^{(q_0 z')} + A_1 \times e^{(q_0 z' + i\theta)} + A_{-1} \times e^{(q_{-1} z' - i\theta)}\right\} \quad (13a)$$

$$v'(\theta, z') = Imag\left\{A_0 \times e^{(q_0 z')} + A_1 \times e^{(q_0 z' + i\theta)} + A_{-1} \times e^{(q_{-1} z' - i\theta)}\right\} \quad (13b)$$

where (u', v') = frictional components of the wind velocity; $q_1 = -(1+i)(\gamma + \sqrt{\alpha\beta_a - \phi})^{1/2}$; $q_{-1} = -(1+i)(-\gamma + \sqrt{\alpha\beta_a - \phi})^{1/2}$; $q_0 = -\left(\alpha\beta_a\right)^{1/4}$; $\alpha = \xi_g / 2K$; $\beta_a = \xi_{ag} / 2K$; $\xi_g = 2v_{\theta g}/r + f$ is the absolute angular velocity; $\xi_{ag} = \partial v_{\theta g}/\partial r + v_{\theta g}/r + f$ is the vertical component of absolute vorticity of the gradient wind; K = the turbulent diffusivity assumed to be constant in this study; $\gamma = v_{\theta g}/2Kr$; $\phi = (1/2Kr)\partial v_{\theta g}/\partial\theta$; and z' = new vertical coordinate used as the base of the computation scheme where $z' = 0$ is located above z_{10} [43]. The other necessary parameters needed for the simulation can be acquired in [51, 52].

3. Model Validation

The hurricane simulation process starts with a selected year, and the number of hurricanes in that year is drawn from the negative binomial distribution [Fig. 3(b)]. The initial parameters for the simulated hurricane, namely initial location (as shown in Fig. 2), heading angle, translational speed

and hurricane intensity, are randomly generated from the HURDAT2 database [6, 7, 25-28, 32]. The trajectory path of a hurricane realization can be obtained using the translation model together with intensity model. A database of synthetic hurricanes corresponding to 10,000 year simulations for hazard and risk analyses has been developed based on the hurricane track model coupled with boundary-layer wind model discussed in Sect. 2.

To validate the abovementioned simulation procedure, the simulated hurricanes will be compared with the historical ones from the HURDAT2 database in the proximity of 48 mileposts along the US Atlantic coastline. This validation approach has been originally proposed by [50] and adopted by [14], where the intensity, translation speed and heading angle of a simulated hurricane that enters into the 250 km region of a coastal milepost are recorded [14, 18, 54]. Since the exact locations of the mileposts are not fully available [55], a group of mileposts covering the entire US Atlantic coastline are redefined as depicted in Fig. 7(a) [6, 7, 25-28, 32]. The simulation results are presented in Fig. 7(b), and good agreement between the simulated and historical hurricanes in terms of annual occurrence rate, intensity, translation speed and heading angle is achieved. This observation suggests that the hurricane simulation framework developed in Sect. 2 is a viable approach for hurricane wind risk assessment.

(a)

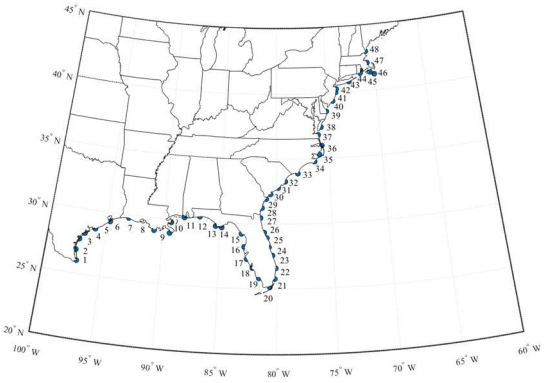

(b)

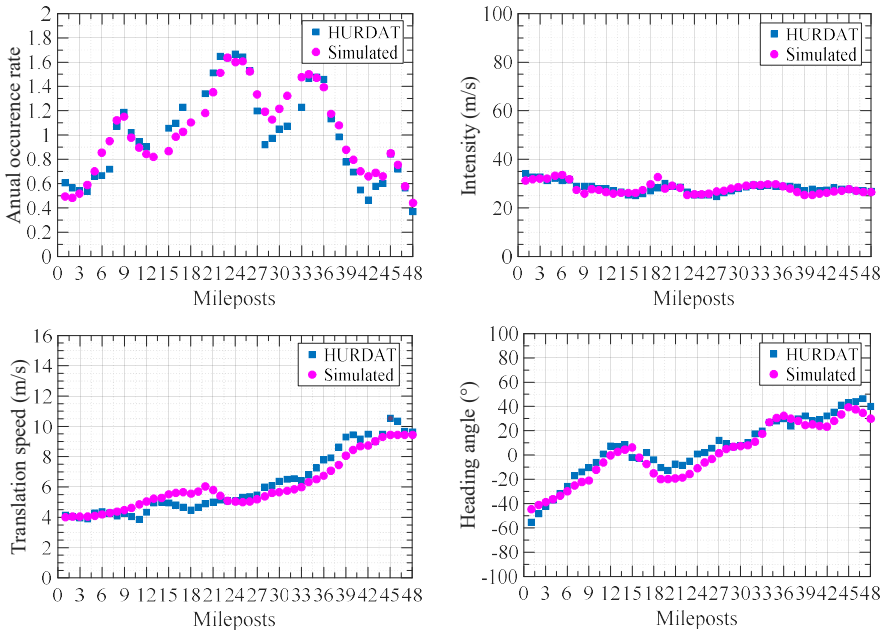

Fig. 7. Validation of simulated hurricanes: (a) mileposts along Atlantic coastline; (b) comparison of simulated and historical hurricanes

4. Case Study

Fourteen locations along the New Jersey coastline are selected as shown in Fig. 8 to apply the developed hurricane simulation framework for wind risk assessment. An example of 50 synthetic hurricane tracks recorded at points 4 and 10 is presented in Fig. 9.

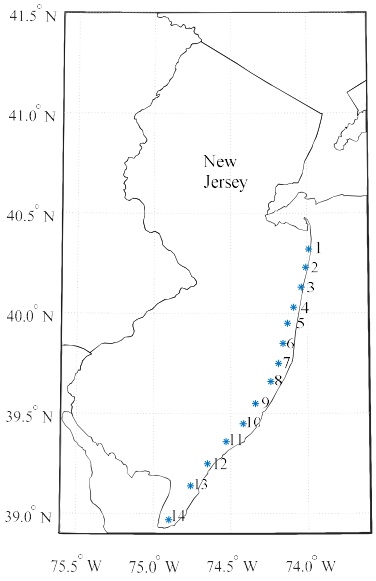

Fig. 8. Selected locations along New Jersey coastline

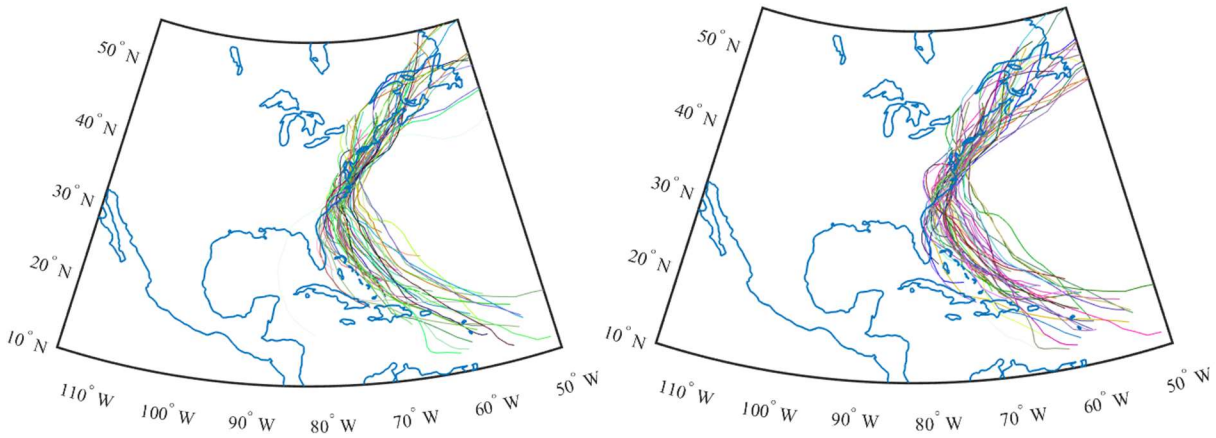

Fig. 9. Tracks of 50 synthetic hurricane recorded at point 4 (left) and point 10 (right)

4.1. Wind speed for various mean recurrence intervals

The mean recurrence interval (MRI) or return period of a given wind speed V_m at a selected site can be determined as [25-28]:

$$MRI\left(v_i > V_m\right) = \frac{1}{\lambda P\left(v_i > V_m\right)} = \frac{Y}{m} \tag{14}$$

where $P\left(v_i > V_m\right)$ = probability that the maximum wind speed v_i is larger than V_m; λ = mean annual occurrence rate of hurricanes at the selected site; and m = number of storms with a maximum wind speed v_i larger than V_m in Y years (i.e., 10,000 years). The MRI distribution of wind speed at two selected points, namely Points 4 and 10 is depicted with a logarithmic scale in Fig. 10.

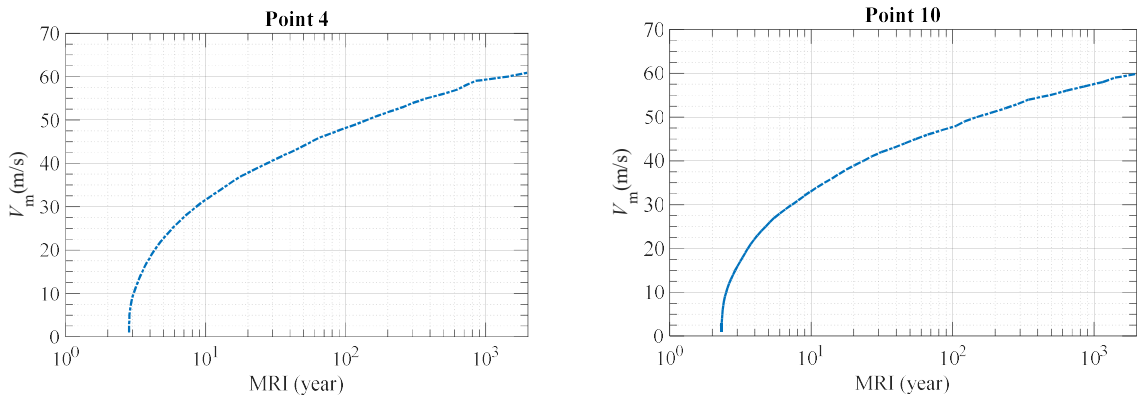

Fig. 10. MRI distribution of wind speed [at 10 m height] at points 4 and 10

The obtained design wind speeds associated with various MRIs [i.e., 10, 25, 50, 100, 300 (risk category I), 700 (risk category II), and 1,700 (risk category III & IV) years] are then compared to the corresponding ones provided by ASCE 7-16. The comparison results at two locations (i.e., points 4 and 10) along the New Jersey coastline are presented in Fig. 11. Good agreement between the simulated and ASCE 7-16 design wind speeds are generally achieved. Differences noticed at several MRIs values (e.g., MRIs of 100, 300 and 700 years at point 4) is due partially to different wind field models used in these two approaches. Since the wind speeds associated with small MRIs (e.g., 10 years) are governed by extratropical cyclones (Nor'easters), the corresponding design wind speed based on the proposed hurricane simulation framework is underestimated. The design wind speeds of the 14 selected points along the New Jersey coastline [Fig. 8] are also plotted in Fig. 12 for two MRIs of 25 and 1700 years. Good agreement between the simulated and ASCE 7-16 design wind speeds is highlighted.

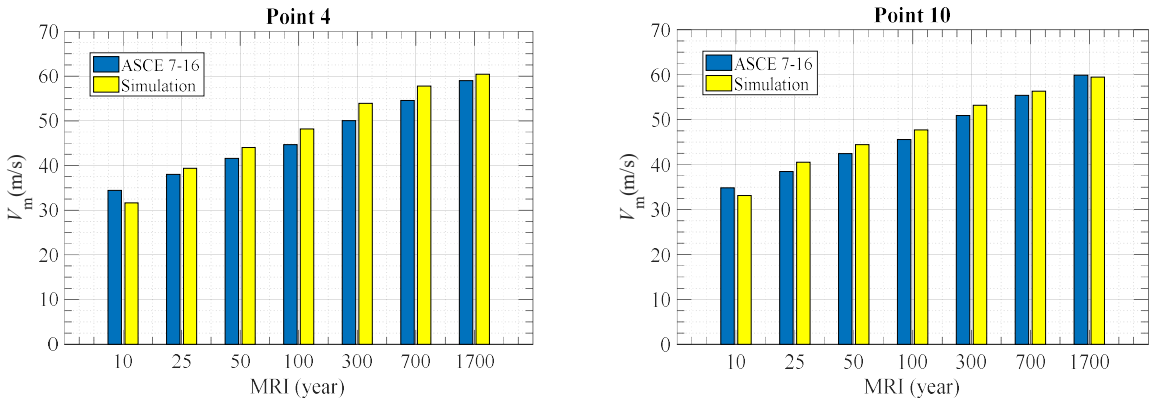

Fig. 11. Comparison of simulated and ASCE 7-16 design wind speeds for various MRIs

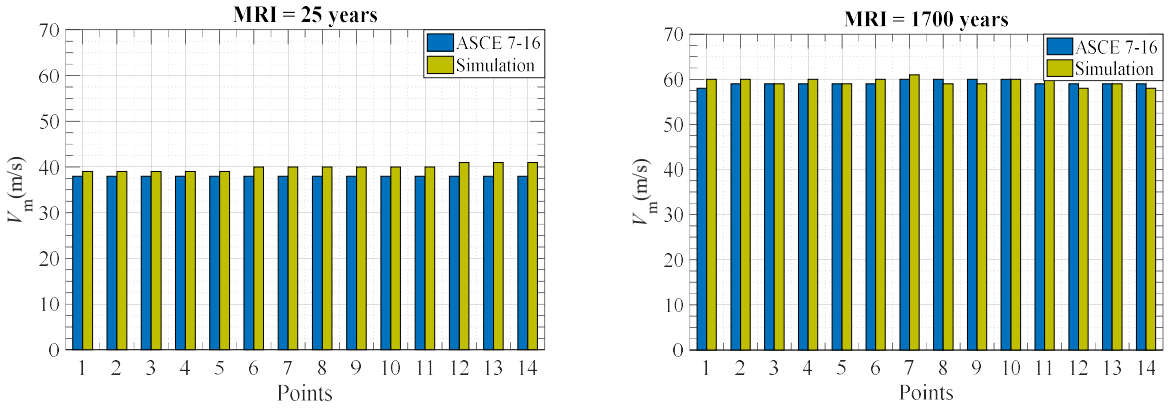

Fig. 12. Comparison of simulated and ASCE 7-16 design wind speeds of 14 selected points

In addition to the surface wind speed as in ASCE 7-16, the developed hurricane simulation framework can provide vertical wind profile since the track model is coupled with an analytical, height-resolving wind field model. An example of simulated vertical wind profiles associated with various MRIs at point 4 and 10 are presented in Fig. 13. It should be noted that the widely-used power-law or log-law wind profiles may be inappropriate to characterize the hurricane boundary-layer winds due to the existence of the supergradient wind region [56-60]. This observation may have significant implications to the wind design of tall buildings.

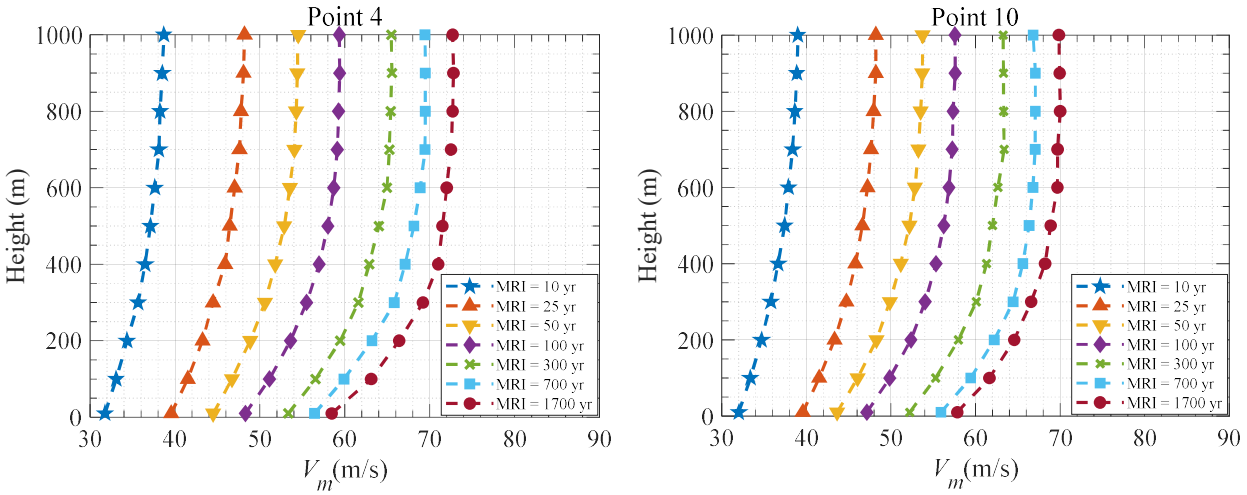

Fig. 13. Vertical wind profiles associated with various MRIs

4.2. Directional design wind speed

The wind directionality is another important factor in the estimation of wind load effects on the structures, whereas ACSE 7-16 only provides the design wind speed. Figure 14 presents the joint distribution histogram of simulated wind speed and direction at two selected points (points 4 and 10). The wind direction convention adopted in this study is that the $0°$ corresponds to wind blowing towards East direction, the $180°$ is for West direction, and the $90°$ is for North direction. As shown in Fig. 14, more hurricane realizations are recorded between $200°$ and $300°$ with an average wind speed generally lower than that between $20°$ and $160°$.

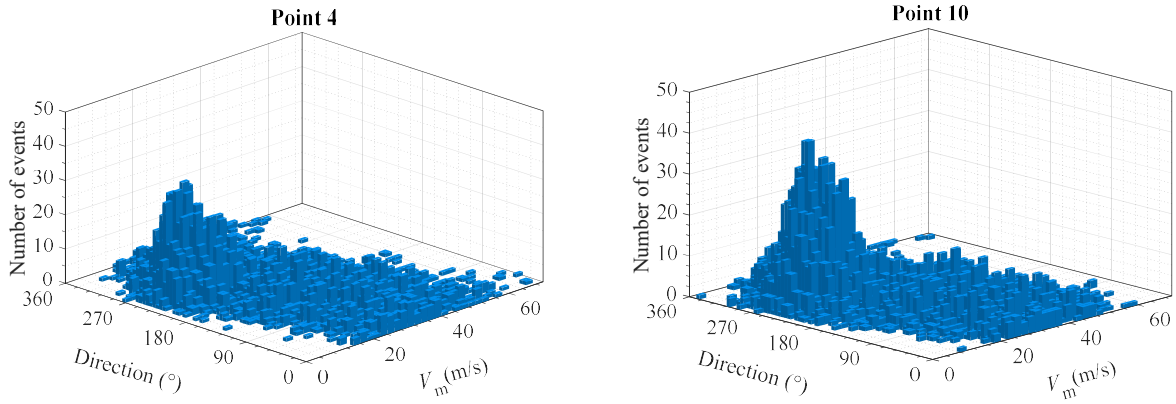

Fig. 14. Joint distribution of hurricane wind speed and direction

The directional maximum wind speeds for various MRIs in each of 16 directional sectors are compared to ASCE 7-16 recommendations, as presented in Fig. 15. It is noted that the simulated design wind speeds for different directional sectors present large variability. Furthermore, the simulation results in Fig. 15 indicates that the ratio between the simulated and ASCE 7-16 design wind speeds depends on the MRI. It is noted that there is a unique value of the directionality factor recommended for each type of structures in ASCE 7-16 to account for a combination effect from the reduced probability of maximum winds coming from any given direction and the reduced probability of the maximum pressure coefficient occurring for any given wind direction [61, 62]. Hence, the information on hurricane wind speed and direction at each site along with the building aerodynamics data (obtained from wind tunnel tests or numerical simulations) may offer an improved wind load estimation.

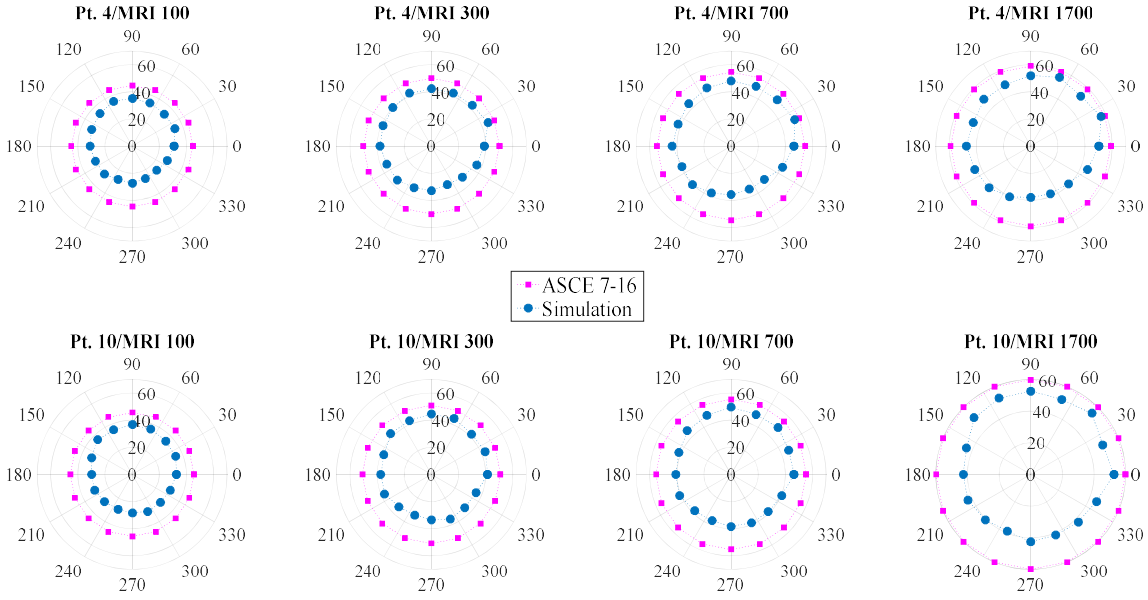

Fig. 15. Comparison of simulated directional design wind speeds and ASCE 7-16 recommendations

4.3. Joint distribution of hurricane wind speed and size

The hurricane size (in terms of the radius of maximum winds $R_{\max}$) significantly affect the likelihood of experiencing strong winds for a given site [56]. It also governs the extent of storm

surge flooding of the landfalling hurricanes that cause widespread damage to property and life [63, 64]. Therefore, the joint histogram of the hurricane wind speed and size is important to be considered [27, 65], and it can be efficiently obtained based on the hurricane simulation framework developed in this study. Figure 16 presents the obtained joint histogram of the hurricane wind speed and size for points 4 and 10.

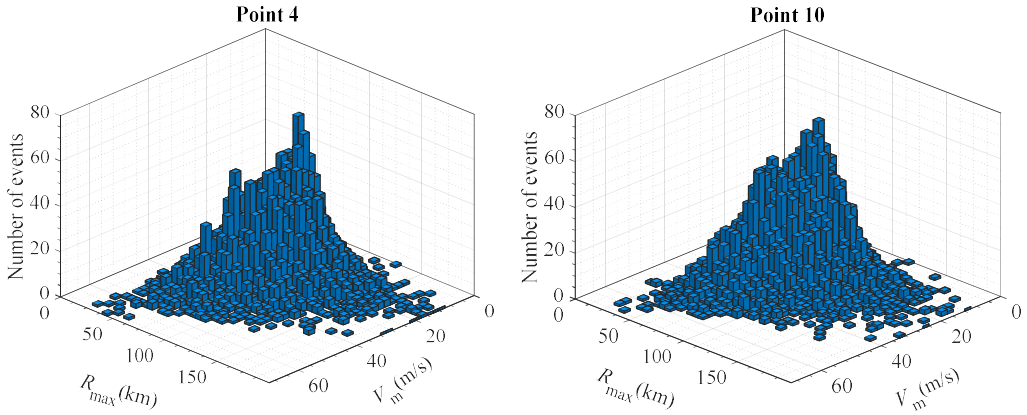

Fig. 16. Joint histogram of hurricane wind speed and size at points 4 and 10

Using the joint histogram in Fig. 16, the joint annual exceedance probability of hurricane wind speed and size can be determined as [65, 66]:

$$P\left(v_i > V_m \cap r_i > R_{\max}\right) = 1 - \sum_{x=0}^{\infty} P\left(v_i \le V_m \cup r_i \le R_{\max} \middle| x\right) p(x) \tag{15a}$$

where $p(x)$ = probability of a number of x hurricanes occurring in a period of one year. Assuming a Poisson distribution of $p(x)$, Eq. (15a) can be rewritten as [65, 66]:

$$P\left(v_i > V_m \cap r_i > R_{\max}\right) = 1 - \exp\left(-n/Y\right) \tag{15b}$$

where n = total number of hurricanes in Y years (i.e., 10,000 years). Figure 17 depicts the joint annual exceedance probability of hurricane wind speed and size for points 4 and 10. The simulation results indicate that points 4 and 10 mostly experience hurricane with $R_{\max}$ of 35-90 km and V_m of 12-34 m/s.

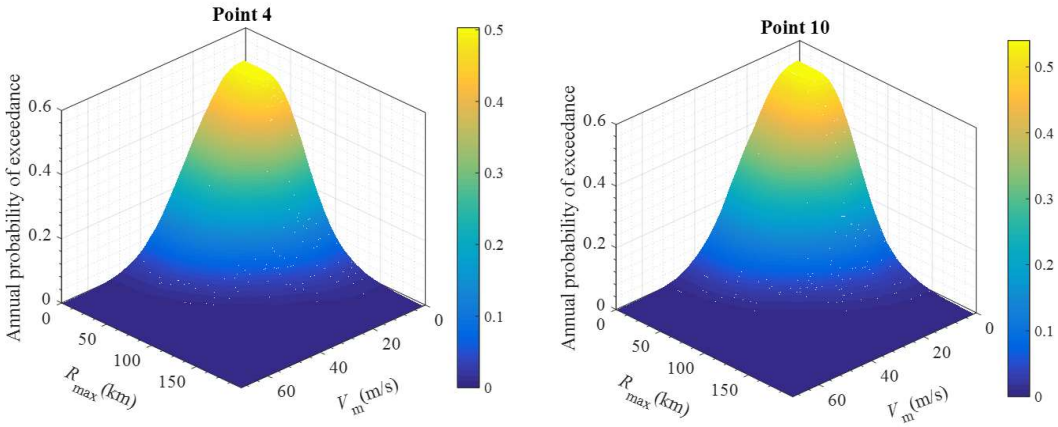

Fig. 17. Joint annual exceedance probability of hurricane wind speed and size at points 4 and 10

Furthermore, the MRI for joint hurricane wind speed and size can be simply constructed as:

$$MRI\left(v_i > V_m \cap r_i > R_{\max}\right) = \frac{1}{\lambda P\left(v_i > V_m \cap r_i > R_{\max}\right)} \tag{16}$$

The results for points 4 and 10 are summarized in Table 1. As discussed in [65], the obtained MRIs for various storm wind speed and size groups can be employed for an improved risk assessment of concomitant hurricane hazards (e.g., wind and surge).

Table 1. MRI for joint hurricane wind speed and size at points 4 and 10

$R_{\max}(km)$	$V_m(m/s)$									
	20		30		40		50		60	
	Pt. 4	Pt. 10	Pt. 4	Pt. 10	Pt. 4	Pt. 10	Pt. 4	Pt. 10	Pt. 4	Pt. 10
10	4.33	3.63	8.59	7.44	27.48	23.81	142.09	150.91	1442.78	2154.49
20	4.33	3.63	8.59	7.44	27.48	23.85	142.09	152.68	1442.78	2154.49
30	4.35	3.65	8.63	7.52	27.73	24.14	144.92	160.19	1803.29	3231.41
40	4.51	3.79	9.04	7.94	29.62	25.94	164.59	172.95	2404.15	4308.33
50	4.90	4.19	10.18	9.10	35.81	30.08	203.82	235.61	14421.32	-
60	5.81	5.00	12.62	11.25	46.07	39.22	289.13	349.91	-	-
70	7.36	6.47	16.82	15.37	64.53	56.83	451.36	616.03	-	-
80	10.07	9.01	24.17	22.78	93.75	92.30	627.70	1292.95	-	-
90	14.63	13.07	36.24	34.83	147.87	152.68	1109.99	3231.41	-	-
100	22.21	20.62	57.49	58.34	258.23	264.38	2404.15	-	-	-
110	35.55	33.03	93.75	102.40	451.36	517.56	7211.02	-	-	-
120	56.18	53.82	144.92	168.47	721.75	1077.56	-	-	-	-
130	98.82	85.66	278.04	275.60	1311.68	1616.03	-	-	-	-

5. Concluding Remarks

422 The hurricane track model is revisited in this study to advance the wind risk assessment
423 methodology, where a physics-based intensity model simply controlled by a growth term (through
424 inward advection of angular momentum) and a decay term (through frictional forces) is highlighted.
425 The evolution of the normalized hurricane intensity $V_{\max}$ (maximum sustained surface wind speed
426 $v_{\max}$ divided by maximum storm intensity V_{mpi}) explicitly depends on several environmental
427 factors of dominant dynamics and thermodynamics, namely the sea surface temperature, vertical
428 shear and convective instability. Based on the developed hurricane risk assessment framework,
429 10,000 years of full-track synthetic hurricanes are generated and compared with historical
430 hurricane records in terms of annual occurrence rate, intensity, translation speed and heading angle.
431 The comparison results suggest the proposed method is a viable approach for hurricane wind risk
432 assessment. In addition to design wind speeds (at surface) associated with various mean recurrence
433 intervals (MRIs) as in ASCE 7-16, the developed hurricane risk assessment framework can also
434 efficiently provide the vertical profiles of wind speed and direction between the ground-surface
435 and gradient levels, joint distribution of hurricane wind speed and direction, and joint distribution
436 of hurricane wind speed and size. All these risk considerations related to hurricane wind hazard
437 have significant implications to wind design of coastal structures.
438
439 **Acknowledgements**
440 The support for this project provided by the NSF Grant # CMMI 15-37431 is gratefully
441 acknowledged.
442
443 **References**
444 [1] Landsea, C.W., 2000. Climate variability of tropical cyclones: past, present and future. Storms. Routledge, New
445 York, pp.220-241.
446 [2] Rappaport, E.N., 2000. Loss of life in the United States associated with recent Atlantic tropical cyclones. Bulletin

of the American Meteorological Society, 81(9), pp.2065-2073.

[3] Knutson, T.R., McBride, J.L., Chan, J., Emanuel, K., Holland, G., Landsea, C., Held, I., Kossin, J.P., Srivastava, A.K. and Sugi, M., 2010. Tropical cyclones and climate change. Nature Geoscience, 3(3), pp.157-163.

[4] Curtis, K.J. and Schneider, A., 2011. Understanding the demographic implications of climate change: estimates of localized population predictions under future scenarios of sea-level rise. Population and Environment, 33(1), pp.28-54.

[5] Snaiki, R., Wu, T., Whittaker, A., Atkinson, J., 2020. Hurricane wind and storm surge effects on coastal bridges under a changing climate. Transportation Research Record. In press.

[6] Rosowsky, D.V., Mudd, L. and Letchford, C., 2016. Assessing climate change impact on the joint wind-rain hurricane hazard for the northeastern US coastline. In Risk Analysis of Natural Hazards, pp. 113-134. Springer, Cham.

[7] Rosowsky, D.V., 2018. Assessing climate change impacts on hurricane hazards. In Climate Change and Its Impacts, pp. 93-107. Springer, Cham.

[8] Russell, L.R., 1968. Probability distributions for Texas Gulf coast hurricane effects of engineering interest. Ph.D. Thesis, Stanford University, Stanford, California, USA.

[9] Russell, L.R., 1971. Probability distributions for hurricane effects. J. Waterw. Harb. Coast Eng. Div. 97 (1), pp. 139–154.

[10] Tryggvason, B.V., Davenport, A.G. and Surry, D., 1976. Predicting wind-induced response in hurricane zones. Journal of the Structural Division, 102(12), pp.2333-2350.

[11] Batts, M.E., Simiu, E. and Russell, L.R., 1980. Hurricane wind speeds in the United States. Journal of the Structural Division, 106(10), pp.2001-2016.

[12] Vickery, P.J. and Twisdale, L.A., 1995. Prediction of hurricane wind speeds in the United States. Journal of Structural Engineering, 121(11), pp.1691-1699.

[13] Emanuel, K., Ravela, S., Vivant, E. and Risi, C., 2006. A statistical deterministic approach to hurricane risk assessment. Bulletin of the American Meteorological Society, 87(3), pp.299-314.

[14] Vickery, P.J., Skerlj, P.F. and Twisdale, L.A., 2000. Simulation of hurricane risk in the US using empirical track model. Journal of Structural Engineering, 126(10), pp.1222-1237.

[15] Powell, M., Soukup, G., Cocke, S., Gulati, S., Morisseau-Leroy, N., Hamid, S., Dorst, N. and Axe, L., 2005. State of Florida hurricane loss projection model: Atmospheric science component. Journal of Wind Engineering and Industrial Aerodynamics, 93(8), pp.651-674.

[16] Hall, T.M. and Jewson, S., 2007. Statistical modelling of North Atlantic tropical cyclone tracks. Tellus A: Dynamic Meteorology and Oceanography, 59(4), pp.486-498.

[17] Lee, K.H. and Rosowsky, D.V., 2007. Synthetic hurricane wind speed records: development of a database for hazard analyses and risk studies. Natural Hazards Review, 8(2), pp.23-34.

[18] Vickery, P.J., Wadhera, D., Twisdale Jr, L.A. and Lavelle, F.M., 2009. US hurricane wind speed risk and uncertainty. Journal of Structural Engineering, 135(3), pp.301-320.

[19] Hong, H.P., Li, S.H. and Duan, Z.D., 2016. Typhoon wind hazard estimation and mapping for coastal region in mainland China. Natural Hazards Review, 17(2), p.04016001.

[20] Chen, Y. and Duan, Z., 2018. A statistical dynamics track model of tropical cyclones for assessing typhoon wind hazard in the coast of southeast China. Journal of Wind Engineering and Industrial Aerodynamics, 172, pp.325-340.

[21] Cui, W. and Caracoglia, L., 2019. A new stochastic formulation for synthetic hurricane simulation over the North Atlantic Ocean. Engineering Structures, 199, p.109597.

[22] Kim, G.Y. and Lee, S., 2019. Prediction of extreme wind by stochastic typhoon model considering climate change. Journal of Wind Engineering and Industrial Aerodynamics, 192, pp.17-30.

[23] Emanuel, K., DesAutels, C., Holloway, C. and Korty, R., 2004. Environmental control of tropical cyclone

493 intensity. Journal of the Atmospheric Sciences, 61(7), pp.843-858.

494 [24] Zhang, S. and Nishijima, K., 2012. Statistics-based investigation on typhoon transition modeling. In The Seventh
495 International Colloquium on Bluff Body Aerodynamics and Applications (BBAA7), Shanghai, China, September
496 2-6.

497 [25] Mudd, L., Wang, Y., Letchford, C. and Rosowsky, D., 2014. Assessing climate change impact on the US East
498 Coast hurricane hazard: temperature, frequency, and track. Natural Hazards Review, 15(3), p.04014001.

499 [26] Mudd, L., Wang, Y., Letchford, C. and Rosowsky, D., 2014. Assessing the impact of climate change on the US
500 east coast hurricane hazard: wind and rain. In Structures Congress 2014, pp. 1426-1436.

501 [27] Mudd, L., Wang, Y., Letchford, C. and Rosowsky, D., 2014. Hurricane wind hazard assessment for a rapidly
502 warming climate scenario. Journal of Wind Engineering and Industrial Aerodynamics, 133, pp.242-249.

503 [28] Mudd, L., Rosowsky, D., Letchford, C. and Lombardo, F., 2017. Joint probabilistic wind–rainfall model for
504 tropical cyclone hazard characterization. Journal of Structural Engineering, 143(3), p.04016195.

505 [29] Jarvinen, B.R., Neumann, C.J. and Davis, M.A.S., 1984. A tropical cyclone data tape for the North Atlantic Basin,
506 1886–1983: Contents, limitations. and uses. Tech. Memo. NWS NHC 22, National Oceanic and Atmospheric
507 Administration.

508 [30] Landsea, C., Franklin, J. and Beven, J., 2015. The revised Atlantic hurricane database (HURDAT2). United States
509 National Oceanic and Atmospheric Administration's National Weather Service. [Available at http://www. nhc.
510 noaa. gov/data/hurdat/hurdat2-format-atlantic. pdf.].

511 [31] Liu, F. and Pang, W., 2013. Influence of climate change on future hurricane wind hazards along the US eastern
512 coast and the Gulf of Mexico. In Advances in Hurricane Engineering: Learning from Our Past, pp. 573-584.

513 [32] Wang, Y. and Rosowsky, D.V., 2018. Hazard-based regional loss estimation considering hurricane intensity, size
514 and sea surface temperature change. Sustainable and Resilient Infrastructure, 3(4), pp.151-164.

515 [33] Akaikei, H., 1973. Information theory and an extension of maximum likelihood principle. In Proc. 2nd Int. Symp.
516 on Information Theory, pp. 267-281.

517 [34] Hurvich, C.M. and Tsai, C.L., 1989. Regression and time series model selection in small samples. Biometrika,
518 76(2), pp.297-307.

519 [35] DeMaria, M., Mainelli, M., Shay, L.K., Knaff, J.A. and Kaplan, J., 2005. Further improvements to the statistical
520 hurricane intensity prediction scheme (SHIPS). Weather and Forecasting, 20(4), pp.531-543.

521 [36] DeMaria, M., 2009. A simplified dynamical system for tropical cyclone intensity prediction. Monthly Weather
522 Review, 137(1), pp.68-82.

523 [37] Darling, R.W.R., 1991. Estimating probabilities of hurricane wind speeds using a large-scale empirical
524 model. Journal of Climate, 4(10), pp.1035-1046.

525 [38] Emanuel, K.A., 1988. The maximum intensity of hurricanes. Journal of the Atmospheric Sciences, 45(7),
526 pp.1143-1155.

527 [39] DeMaria, M. and Kaplan, J., 1994. Sea surface temperature and the maximum intensity of Atlantic tropical
528 cyclones. Journal of Climate, 7(9), pp.1324-1334.

529 [40] Zeng, Z., Wang, Y. and Wu, C.C., 2007. Environmental dynamical control of tropical cyclone intensity - An
530 observational study. Monthly Weather Review, 135(1), pp.38-59.

531 [41] Xu, J., Wang, Y. and Tan, Z.M., 2016. The Relationship between Sea Surface Temperature and Maximum
532 Intensification Rate of Tropical Cyclones in the North Atlantic. Journal of the Atmospheric Sciences, 73(12),
533 pp.4979-4988.

534 [42] Vogl, S., 2009. Tropical cyclone boundary-layer models. Ph.D. Thesis, Ludwig Maximilians University Munich,
535 Munich.

536 [43] Meng, Y., Matsui, M. and Hibi, K., 1995. An analytical model for simulation of the wind field in a typhoon
537 boundary layer. Journal of Wind Engineering and Industrial Aerodynamics, 56(2-3), pp.291-310.

538 [44] Simpson, J. and Wiggert, V., 1969. Models of precipitating cumulus towers. Mon. Wea. Rev, 97(7), pp.471-489.

539 [45] Reynolds, R.W., Rayner, N.A., Smith, T.M., Stokes, D.C. and Wang, W., 2002. An improved in situ and satellite
540 SST analysis for climate. Journal of Climate, 15(13), pp.1609-1625.

541 [46] Powell, M.D., Vickery, P.J. and Reinhold, T.A., 2003. Reduced drag coefficient for high wind speeds in tropical
542 cyclones. Nature, 422(6929), po.279–283.

543 [47] Kaplan, J. and DeMaria, M., 1995. A simple empirical model for predicting the decay of tropical cyclone winds
544 after landfall. Journal of Applied Meteorology, 34(11), pp.2499-2512.

545 [48] Kaplan, J. and DeMaria, M., 2001. On the decay of tropical cyclone winds after landfall in the New England
546 area. Journal of Applied Meteorology, 40(2), pp.280-286.

547 [49] DeMaria, M., Knaff, J.A. and Kaplan, J., 2006. On the decay of tropical cyclone winds crossing narrow
548 landmasses. Journal of Applied Meteorology and Climatology, 45(3), pp.491-499.

549 [50] Georgiou, P.N., 1986. Design wind speeds in tropical cyclone-prone regions. PhD Thesis, University of Western
550 Ontario, London, Ontario, Canada.

551 [51] Snaiki, R. and Wu, T., 2017. Modeling tropical cyclone boundary layer: Height-resolving pressure and wind fields.
552 Journal of Wind Engineering and Industrial Aerodynamics, 170, pp.18-27.

553 [52] Snaiki, R. and Wu, T., 2017. A linear height-resolving wind field model for tropical cyclone boundary layer.
554 Journal of Wind Engineering and Industrial Aerodynamics, 171, pp.248-260.

555 [53] Vickery, P.J. and Wadhera, D., 2008. Statistical models of Holland pressure profile parameter and radius to
556 maximum winds of hurricanes from flight-level pressure and H* Wind data. Journal of Applied Meteorology and
557 climatology, 47(10), pp.2497-2517.

558 [54] Liu, F., 2014. Projections of future US design wind speeds due to climate change for estimating hurricane losses.
559 PhD Thesis. Clemson University, USA.

560 [55] Cui, W. and Caracoglia, L., 2016. Exploring hurricane wind speed along US Atlantic coast in warming climate
561 and effects on predictions of structural damage and intervention costs. Engineering Structures, 122, pp.209-225.

562 [56] Vickery, P.J., Wadhera, D., Powell, M.D. and Chen, Y., 2009. A hurricane boundary layer and wind field model
563 for use in engineering applications. Journal of Applied Meteorology and Climatology, 48(2), pp.381-405.

564 [57] Snaiki, R. and Wu, T., 2018. A semi-empirical model for mean wind velocity profile of landfalling hurricane
565 boundary layers. Journal of Wind Engineering and Industrial Aerodynamics, 180, pp.249-261.

566 [58] Snaiki, R. and Wu, T., 2019. Knowledge-enhanced deep learning for simulation of tropical cyclone boundary-
567 layer winds. Journal of Wind Engineering and Industrial Aerodynamics, 194, p.103983.

568 [59] Snaiki, R. and Wu, T., 2020. An analytical model for rapid estimation of hurricane supergradient winds. Journal
569 of Wind Engineering and Industrial Aerodynamics, 201, p.104175.

570 [60] Snaiki, R., 2020. Rapid Estimate of Hurricane Wind, Rain and Storm Surge under Changing Climate. PhD Thesis.
571 State University of New York at Buffalo, USA.

572 [61] Laboy-Rodríguez, S.T., Gurley, K.R. and Masters, F.J., 2014. Revisiting the directionality factor in ASCE 7.
573 Journal of Wind Engineering and Industrial Aerodynamics, 133, pp.225-233.

574 [62] McAllister, T.P., Wang, N. and Ellingwood, B.R., 2018. Risk-Informed Mean Recurrence Intervals for Updated
575 Wind Maps in ASCE 7-16. Journal of Structural Engineering (New York, NY), 144(5).

576 [63] Irish, J.L., Resio, D.T. and Ratcliff, J.J., 2008. The influence of storm size on hurricane surge. Journal of Physical
577 Oceanography, 38(9), pp.2003-2013.

578 [64] Uhlhorn, E.W., Klotz, B.W., Vukicevic, T., Reasor, P.D. and Rogers, R.F., 2014. Observed hurricane wind speed
579 asymmetries and relationships to motion and environmental shear. Monthly Weather Review, 142(3), pp.1290-
580 1311.

581 [65] Wang, Y. and Rosowsky, D.V., 2012. Joint distribution model for prediction of hurricane wind speed and size.
582 Structural Safety, 35, pp.40-51.

583 [66] Pei, B., Pang, W., Testik, F.Y., Ravichandran, N. and Liu, F., 2014. Mapping joint hurricane wind and surge
584 hazards for Charleston, South Carolina. Natural Hazards, 74(2), pp.375-403.

585